ARTICLE

OPEN ACCESS

www.the-innovation.org

Thalamic burst and tonic firing selectively indicate patients' consciousness level and recovery

Huan Wang,[1,2,10] Yongxiang Hu,[1,3,10] Qianqian Ge,[4] Yuanyuan Dang,[5] Yi Yang,[4] Long Xu,[4] Xiaoyu Xia,[5] Peng Zhang,[1,2] Sheng He,[1,2,6] Steven Laureys,[7,8,9] Yan Yang,[1,2,*] and Jianghong He[4,*]

*Correspondence: yyang@ibp.ac.cn (Y.Y.); he_jianghong@sina.cn (J.H.)

Received: December 21, 2024; Accepted: February 24, 2025; Published Online: February 25, 2025; https://doi.org/10.1016/j.xinn.2025.100846

GRAPHICAL ABSTRACT

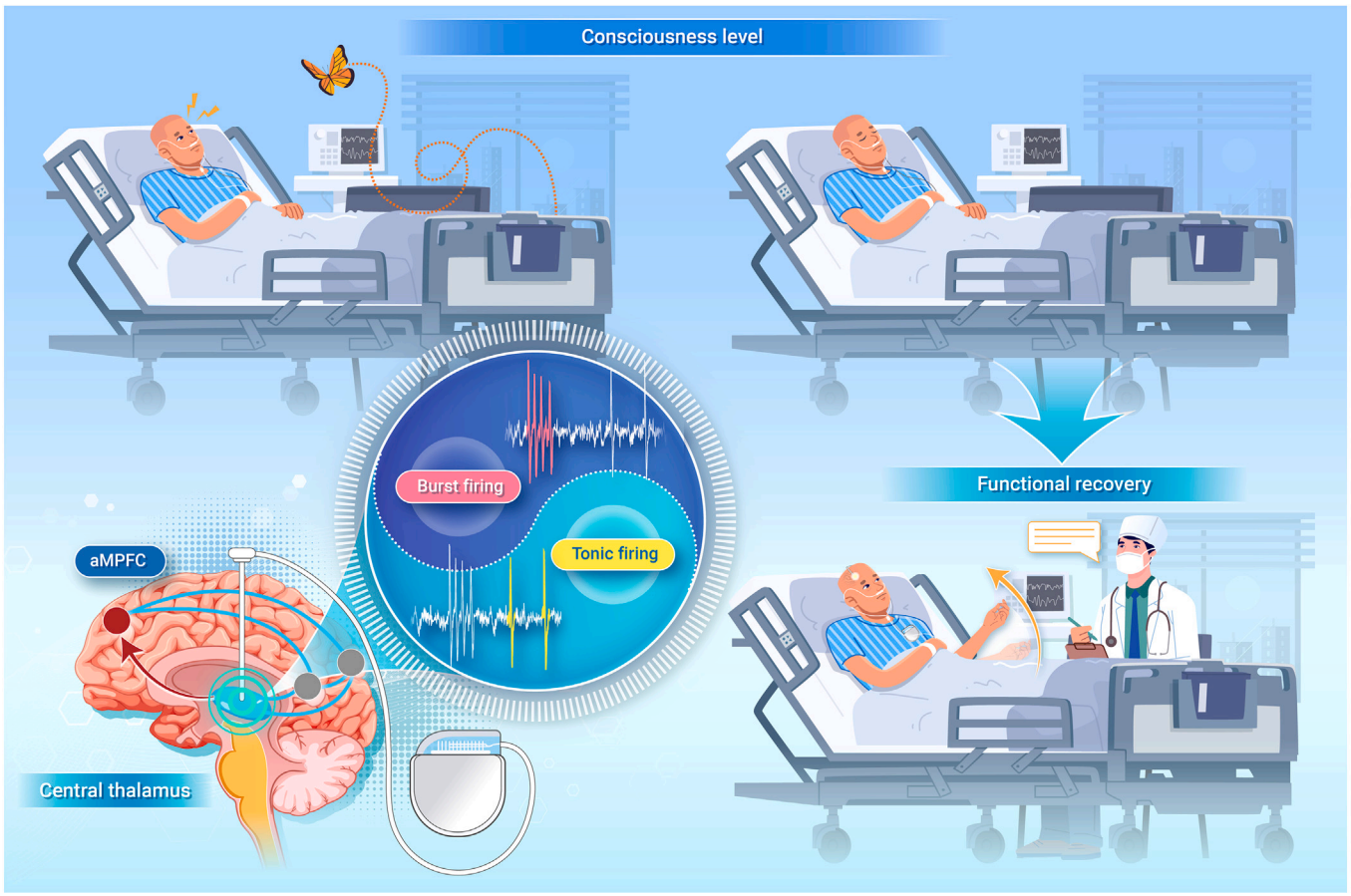

PUBLIC SUMMARY

- Thalamic spike analyses are conducted in 29 patients with disorders of consciousness.
- Thalamic tonic and burst firing modes distinctly signal consciousness level and recovery.
- Burst firing reflects consciousness; minimally conscious ones show shorter, stable bursts.
- Tonic firing in centromedian/parafascicular nuclei predicts deep brain stimulation outcome.

OPEN ACCESS

ARTICLE

The Innovation

Thalamic burst and tonic firing selectively indicate patients' consciousness level and recovery

Huan Wang,[1,2,10] Yongxiang Hu,[1,3,10] Qianqian Ge,[4] Yuanyuan Dang,[5] Yi Yang,[4] Long Xu,[4] Xiaoyu Xia,[5] Peng Zhang,[1,2] Sheng He,[1,2,6] Steven Laureys,[7,8,9] Yan Yang,[1,2,*] and Jianghong He[4,*]

[1]State Key Laboratory of Cognitive Science and Mental Health, Institute of Biophysics, Chinese Academy of Sciences, Beijing 100101, China
[2]University of Chinese Academy of Sciences, Beijing 100049, China
[3]School of Life Science, University of Science and Technology of China, Hefei 230027, China
[4]Department of Neurosurgery, Beijing Tiantan Hospital, Capital Medical University, Beijing 100070, China
[5]Department of Neurosurgery, First Medical Center of Chinese PLA General Hospital, Beijing 100039, China
[6]Institute of Artificial Intelligence, Hefei Comprehensive National Science Center, Hefei 230088, China
[7]CERVO Brain Research Centre, Laval University, Quebec, QC G1J 2G3, Canada
[8]Coma Science Group, GIGA Consciousness Research Unit, Liège University, 4000 Liège, Belgium
[9]International Consciousness Science Institute, Hangzhou Normal University, Hangzhou 311121, China
[10]These authors contributed equally
*Correspondence: yyang@ibp.ac.cn (Y.Y.); he_jianghong@sina.cn (J.H.)

Received: December 21, 2024; Accepted: February 24, 2025; Published Online: February 25, 2025; https://doi.org/10.1016/j.xinn.2025.100846

Citation: Wang H., Hu Y., Ge Q., et al., (2025). Thalamic burst and tonic firing selectively indicate patients' consciousness level and recovery. The Innovation **6(5)**, 100846.

Patients with disorders of consciousness suffer from severe impairments in arousal and awareness alongside anomalous brain connections and aberrant neuronal activities. The thalamus, a crucial hub in the brain connectome, has been empirically inferred to maintain consciousness and wakefulness. Here, we investigated thalamic spiking, brain connectivity, consciousness states, and recovery outcomes following deep brain stimulation in 29 patients. Our study reveals that thalamic neuronal activity serves as a marker of consciousness state. Patients diagnosed with vegetative state/unresponsive wakefulness syndrome exhibited less-active neurons, with longer and more variable burst discharges, than those in a minimally conscious state. Furthermore, neuronal profiles in the intralaminar thalamus, the direct stimulation site, predicted whether electrostimulation here improved recovery. Stronger tonic firing was correlated with enhanced thalamocortical connectivity and better recovery outcomes in patients. These findings suggest that thalamic spiking signatures, including single-neuron burst discharge and tonic firing, selectively indicate the representation and alteration of consciousness.

INTRODUCTION

The thalamus may modulate consciousness through its spiking activity. Thalamic dual firing modes, tonic and burst, have distinct effects on thalamocortical interactions.[1–7] Their burst modes are regulated during states of unresponsiveness or unconsciousness. Nonetheless, this knowledge about neuronal correlates of consciousness, especially at the cellular level, was derived primarily from comparisons between anesthesia, natural sleep, and wakefulness in animal models (rodents,[8] cats,[9] and monkeys[10]). Data from three patients with disorders of consciousness (DoC) have shown, in only a few clinical cases, that vegetative state/unresponsive wakefulness syndrome (VS/UWS) and minimally conscious state (MCS) differ in thalamic spiking activity.[11] The lack of neurophysiological signature analysis in DoC patients, particularly at the single-unit level, hinders our ability to gain a deeper understanding of the neuronal mechanisms of these disorders.

As the primary hub between the brain-stem arousal nuclei and the cerebral cortex, the thalamus, especially the intralaminar thalamus, may function as an essential node within the neuronal network responsible for regulating arousal.[12–18] The mesocircuit hypothesis posits that the recovery of consciousness may be influenced by frontostriatal connections, with a specific contribution from the thalamus.[12,14] Deep brain stimulation (DBS) targeting the intralaminar thalamus, including the centromedian/parafascicular complex (CM/Pf) and central lateral nucleus (CL), has been demonstrated to improve cognitive and behavioral functions in patients with DoC.[12,14,19–25] In non-human primates, thalamic DBS has been observed to modulate thalamocortical and corticocortical interactions, alter activity in wide-ranging frontoparietal cortices and the cingulate, and even rouse animals from stable anesthesia.[10,26–28] Although stimulation targeting specific nodes and connections could reactivate injured arousal networks and promote the reemergence of consciousness, the underlying neuronal mechanisms and neuronal circuits have not yet been fully elucidated. Furthermore, clinical evidence suggesting variable effects of arousal regulation via DBS among DoC patients[20,29] speaks for personalized prognostic approaches.[30] Future research is required to comprehend intrinsic neuronal mechanisms driving DoC symptoms and their modulation following DBS, particularly through detailed investigations of single-neuron activity and functional connections in patients, supported by direct clinical data.

Here, we conducted a retrospective investigation into the neuronal mechanisms underlying the representation and alteration of consciousness in 29 patients (Table 1) diagnosed with DoC. We employed multimodal measurements utilized in clinical treatments. Specifically, we analyzed thalamic spiking activity that was collected while patients were recovering from anesthesia during neurosurgery. We statistically evaluated relationships between the spiking activity of thalamic neurons, preoperative resting-state functional magnetic resonance imaging (rs-fMRI) data, and clinical neurobehavioral assessments before and after DBS within a 12-month period (Figure S1A).

MATERIALS AND METHODS

DoC patients

This retrospective research included a total of 29 patients who were confirmed with DoC and received thalamic DBS as their clinical treatment (Figure S1). They were diagnosed with MCS (12 patients) or VS/UWS (17 patients) by neurosurgeons according to Coma Recovery Scale-revised (CRS-R) scores.[31] These patients exhibited prolonged DoC for a minimum of 28 days after brain injury, without serious structural brain damage or abnormalities. The preoperative consciousness states were scored as CRS-R_{T0} (Figure S1A). Follow-up assessments were normally scheduled at four intervals after the DBS surgery: 1 month, 3 months, 6 months, and 12 months. The Glasgow Outcome Scale (GOS)[32] was used as the main prognostic assessment, and the follow-up CRS-R was assessed to monitor consciousness state following DBS.[33] Patients who showed ongoing improvement were evaluated based on the 12-month follow-up outcomes. Data from the most favorable follow-up assessment were considered for patients whose condition deteriorated due to complications. Both GOS and CRS-R scores of patients were assessed by experienced neurosurgeons during the 12-month follow-up assessments (T_{12} in Figure S1A). Table S1 details patients' information. Patients primarily received rehabilitation treatment in accordance with clinical guidelines. Additional interventions were tailored to individual conditions and determined by physicians' assessments, adhering to the recommended protocols. These interventions typically included routine rehabilitation treatments, such as active and passive limb movements, as well as supportive care, including skin management, complication control, and nutritional support.

The clinical dataset analyzed in the study was acquired from DoC patients undergoing clinical treatment at the neurosurgery departments of two hospitals. The study was approved by the ethics committee of Beijing Tiantan Hospital, Capital Medical University (protocol no. KY2017-361-01), and the ethics committee of PLA Army General Hospital (protocol no. 2011-0415). The patients' parents or legal guardian signed two patient consent forms after receiving thorough information and discussion about the treatment processes. One consent form provided comprehensive details about the treatment processes, outlining

Table 1. Demographic data and clinical characteristics of patients

Variable	Value
Age, years, mean (SD)	45.9 (14.3)
Sex (%)	
Female	12 (41.4)
Male	17 (58.6)
Etiology (%)	
Anoxia	13 (44.8)
Trauma	8 (27.6)
Stroke	8 (27.6)
Diagnosis (%)	
MCS	12 (41.4)
VS/UWS	17 (58.6)
Interval since injury, months, mean (SD)	5.1 (3.0)
CRS-R_{T0}, mean (SD)	7.2 (2.5)
GOS, mean (SD)	2.5 (0.8)
CRS-R_{T12}, mean (SD)	10.8 (5.9)

VS/UWS, vegetative state/unresponsive wakefulness syndrome; MCS, minimally conscious state; CRS-R, Coma Recovery Scale-revised total scores; GOS, Glasgow Outcome Scale.

the surgical procedure, accompanying risks, and potential for the treatment to be entirely ineffective. The other consent form pertained to research participation, stating that patients' data obtained before, during, and after surgery (such as MRI, computed tomography [CT], intraoperative thalamic spiking recordings, and behavioral assessments) would be utilized for prospective research analyses. Both consent forms ensured that the patients' parents or legal guardian were fully informed and gave consent to aspects of the treatment and potential prospective research. All clinical data utilized in this study were collected and examined to serve for clinical treatments. There were no extra examinations conducted for research purposes.

Blinding

The collection and analysis of patients' data were conducted by separate groups of investigators in a completely blinded fashion. Investigators from two neurosurgery departments who collected clinical data were blinded to the properties of functional brain connectivity in DoC patients and their full sets of thalamic spiking signatures. Investigators from the Institute of Biophysics who performed the analyses on thalamic spiking profiles and brain connections were blinded to patients' states of consciousness and the outcomes of DBS until they finished all the spiking signatures and brain connections analyses.

MRI acquisition

Prior to surgery (T_0, Figure S1A), patients received rs-fMRI and T1-weighted 3D high-resolution and diffusion MRI scanning. During the MRI scan, no sedatives or anesthetics were administered to the patients. rs-fMRI scans were acquired using a T2-weighted gradient echo sequence, and diffusion MRI scans were acquired using an EP/SE sequence on 3.0-T scanners. Details of scanning information are listed in Table S2.

DBS implantation and reconstruction of lead trajectories during surgery

The surgical planning was designed by Leksell SurgiPlan for utilization with the Leksell stereotactic system (Elekta, Stockholm, Sweden). The anatomical location of the CM/Pf was 7.8–9.7 mm posterior to the middle of the anterior commissural (AC)-posterior commissural (PC) line, 8.8–10.5 mm distal to the AC-PC line (4.5–5.5 mm from the ventricular wall), and 0–1.5 mm inferior to the AC-PC plane.[22] Twenty-seven patients had bilateral implantation of quadripolar DBS leads (Medtronic #3387, USA, or PINS L302, China), while two patients had unilateral implantation, for a grand total of 56 trajectories (Figure S1C). Microelectrode recordings were employed during surgery when patients recovered from anesthesia to help determine the targeting location of the CM/Pf, as this required the use of considerably less distracting background noise and neuronal activities.[22,34] The thalamic activities, as observed through single-unit and multiunit frequencies in our data, exhibited a decrease when microelectrodes were introduced through the ventral lateral nucleus (VL) and CL to the CM/Pf (Figures S1D and S1E). Then, DBS leads were implanted into the thalamus along the same path as the microelectrodes. Standard punctures involved microelectrodes and leads entering the thalamus at the VL, traversing the CL, and aiming for a region between the CM and the Pf (Figure 1B).

To verify the accuracy of their placements, postoperative CT or MRI images were utilized to reconstruct lead trajectories applying Lead-DBS software version 2.5.3 (https://www.lead-dbs.org/).[35] Using Advanced Normalization Tools[36] and Statistical Parametric Mapping (SPM12),[37] respectively, postoperative CT and MRI brain images were co-registered to preoperative MRI. A coarse subcortical mask[38] was applied (as implemented in Lead-DBS) to eliminate bias generated by brain shift that might have occurred during surgery. Images were non-linearly normalized to the Montreal Neurological Institute (MNI; ICBM 2009b non-linear asymmetric) template space using the SyN Diffeomorphic Mapping approach implemented in Advanced Normalization Tools, with the preset "Effective: Low Variance + subcortical refinement" to acquire a most precise subcortical alignment between patients and MNI space. This method was considered to have the best performance on subcortical registrations and was proposed by a recent comparative study[39] that evaluated six different non-linear atlas-based subcortical normalization and segmentation methods and reproduced independently by another study.[40] The trajectories were then reconstructed automatically using the TRAC/CORE approach and manually modified to evaluate the contact points with greater precision. Consequently, lead trajectories were reconstructed and contact coordinates were transformed into MNI space.

DBS stimulation and the volume of tissue activated modeling

The DBS stimulation was administered 7 days after the operation, after the incision had healed and the edema generated by the puncture had subsided. Periodic electrical stimulation was delivered via the C0 contact to the CM/Pf of patients (Figure S1C). The primary stimulation source was monopolar and consisted of 100-Hz, 120-μs, and 3.0- to 4.0-V pulses.[22,41] Continuous stimulation was administered from 8 a.m. to 8 p.m. with a cycle of 15 min on and 15 min off (Figure S1B).

To evaluate effective activation fields of DBS, we simulated the volume of tissue activated (VTA) in patients' native space based on contact configuration and stimulation voltage settings by using a finite element method.[35] A volume conductor model was conducted based on a four-compartment mesh that separated perielectrode tissue into gray matter (nuclei were defined according to the Krauth/Morel thalamic atlas[42]), white matter, electrode conducts, and insulated parts. Then, the activation field distribution was simulated using an adaptation of the FieldTrip-SimBio pipeline implemented in Lead-DBS and transformed into MNI space using the aforementioned normalization warp fields. To define the binary activation field, a threshold of 0.2 V/mm[35] was applied. We simulated activation fields with voltages ranging from 3.0 to 4.0 V and obtained similar results. The data with a voltage setting of 3.5 V are shown in Figure 5A.

Intraoperative microelectrode recordings

Anesthesia with propofol was terminated 30 min prior to recordings during surgery. Microelectrodes with a single channel were used intraoperatively to record neuronal activities (LeadPoint System, Medtronic, USA; Neuro Nav, Alpha Omega, Israel). Signals were sampled at 24 kHz and subjected to hardware-based band-pass filtering (500–5,000 Hz) and notch filtering (50 Hz). Each site was recorded for 10 s. Data acquisitions generally began 10–11 mm above the target and advanced in 0.5-mm steps until reaching a depth of 1–3 mm below the target.

The anatomical positions of recording sites were identified based on their depth in millimeters (relative to the target position) along the lead trajectories reconstructed. This resulted in 3D coordinates for recordings in both brain hemispheres. According to the lowest Euclidean distance between recording sites and masks from the Krauth/Morel thalamic atlas, recording sites were allocated to the thalamic nuclei from whence they originated.[42] A total of 731 recording sites located in the thalamus from 29 individuals were included in the subsequent spike sorting analysis.

Spike sorting

We used a Wave_clus MATLAB tool (https://github.com/csn-le/wave_clus)[43] for spike identification and sorting, employing default parameters throughout the process. The raw recording data were zero-phase filtered with a fourth-order band-pass elliptic filter between 500 and 5,000 Hz. Spikes were detected with an automatic amplitude threshold, which was set as five times the estimated standard deviation of the noise. During the feature extraction phase, wavelet coefficients of each detected spike were retrieved using a four-scale multiresolution decomposition with a Haar wavelet. Ten wavelet coefficients with the greatest capacity for distinguishing different spike waveform shapes were

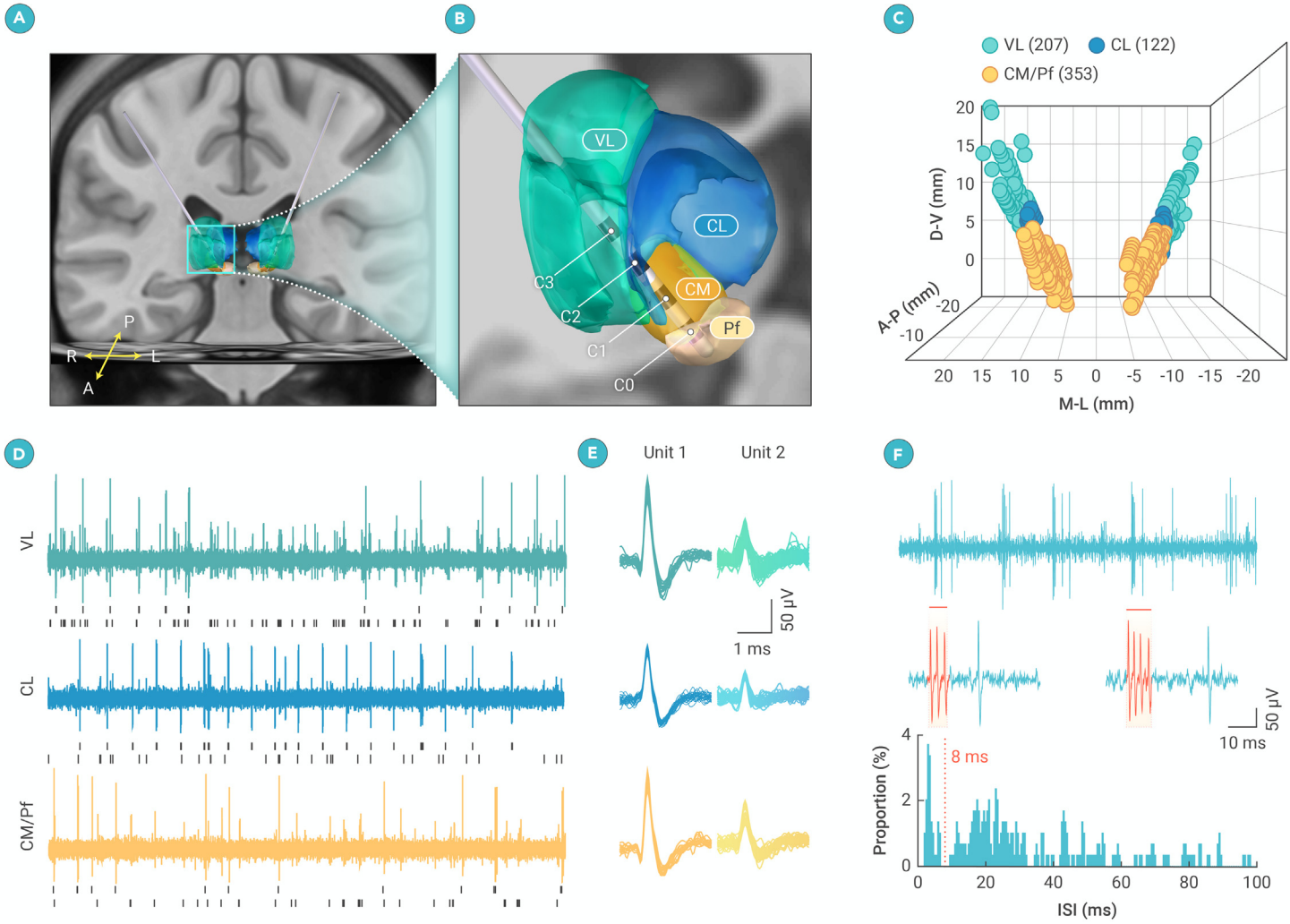

Figure 1. Neuronal spiking recording and DBS applications in the human thalamus (A) Example trajectories in a DoC patient show bilateral implantation of quadripolar DBS leads into the thalamus. A, anterior; P, posterior; R, right; L, left. (B) Magnification of the right hemisphere (blue box in A) shows the anatomical structures of four thalamic nuclei (green, ventral lateral nucleus [VL]; blue, central lateral nucleus [CL]; yellow, centromedian nucleus [CM]; and pink, parafascicular nucleus [Pf]) and the lead contacts' locations. (C) Three-dimensional positions of 682 thalamic recording sites in 29 patients. (D and E) Examples of neuronal spiking activity in the thalamic nuclei from a patient. (D) Raw spike traces of 5 s, with short black lines representing spike trains of sorted neurons. Their spike waveforms are shown in (E). (F) Burst and tonic modes of an example thalamic neuron. From top to bottom: raw spike trace of 1 s, with red bars indicating two burst events; the two bursts shown with an expanded time base (red traces with three and four spikes in each one); and distribution of its ISIs with 15.44% of spikes in bursts defined by an interspike interval of less than 8 ms.

chosen through a Lilliefors modification of the Kolmogorov-Smirnov test of normality. Last, an unsupervised superparamagnetic clustering approach was used to classify spike waveform characteristics into different clusters based on the 11-nearest-neighbor interactions. The main parameter that affects the performance of superparamagnetic clustering is the "temperature." This parameter's range was set from 0 to 0.25 in steps of 0.01. Optimal temperature was determined as the highest temperature at which a cluster contained at least 20 members. We calculated the signal-to-noise ratio of a single unit as the amplitude of mean waveform (trough-to-peak) divided by the standard deviation. The interspike interval violation percentage was also calculated as the percentage of all spikes with interspike interval smaller than 1 ms. Only units with signal-to-noise ratio greater than or equal to 2 and interspike interval violation less than or equal to 1% were used in further analyses. Spikes within a 1-ms interspike interval were removed from spike trains.

Using the spike sorting approach, we gathered 1,016 neurons from a total of 731 thalamic recording sites. Of these, 94.49% (960 of 1,016) exhibited two distinct firing modes, burst and tonic. The subsequent investigations focused on these 960 neurons from 682 sites, at both single-unit and multiunit levels, within the three thalamic nuclei. For *a single neuron*, we analyzed a series of signatures, including the single-unit frequency (SUF) and the geometric coefficient of variation (GCV) of its interspike interval, the firing rates of burst spikes (BS) and tonic spikes (TS), the burst event frequency (BEF, burst events per second), and the burst length (BL, spike numbers per burst) and its coefficient of variation (BL-CV). For *multiple neurons*, we computed the multiunit frequency (MUF), the sample entropy (SpEn), and the unit number (UN) at each recording site. Here, 10 spike-based neuronal signatures were extracted from DoC patients to characterize a panoramic view of neuronal spiking activity in the thalamus. To evaluate neuronal signatures for both single units and multiple units at each recording site without bias toward specific types of thalamic neurons, we performed analyses on the mean responses across neurons when multiple neurons were recorded at that site.

Single unit and multiunits

We evaluated neuronal signatures of the 682 recording sites based on their single-unit and multiunit activities: 207 sites were in the VL (including anterior and posterior subdivisions), 122 sites were in the CL, and 353 sites were in the CM/Pf (Figure 1C). There were multiple neurons recorded at 42.51% (88/207), 31.97% (39/122), and 18.41% (65/353) of the recording sites in these three thalamic nuclei. The single-unit studies included analyses of single-unit frequency, GCV of interspike interval, burst, and tonic activity. In order to mitigate potential bias toward specific types of thalamic neurons at each recording site, we conducted analyses on the mean responses across neurons to present signatures at the single-neuron level if there were multiple units recorded at a given site. The multiunit frequency, unit number, and SpEn were utilized to describe the neuronal signatures of multiple units at that site. The neuronal firing rates were computed by dividing the number of spikes by the recording duration.

Burst and tonic modes

To capture the temporal properties of neuronal firing, we generated the interspike interval histograms with a bin width of 0.5 ms for each single unit using FieldTrip software

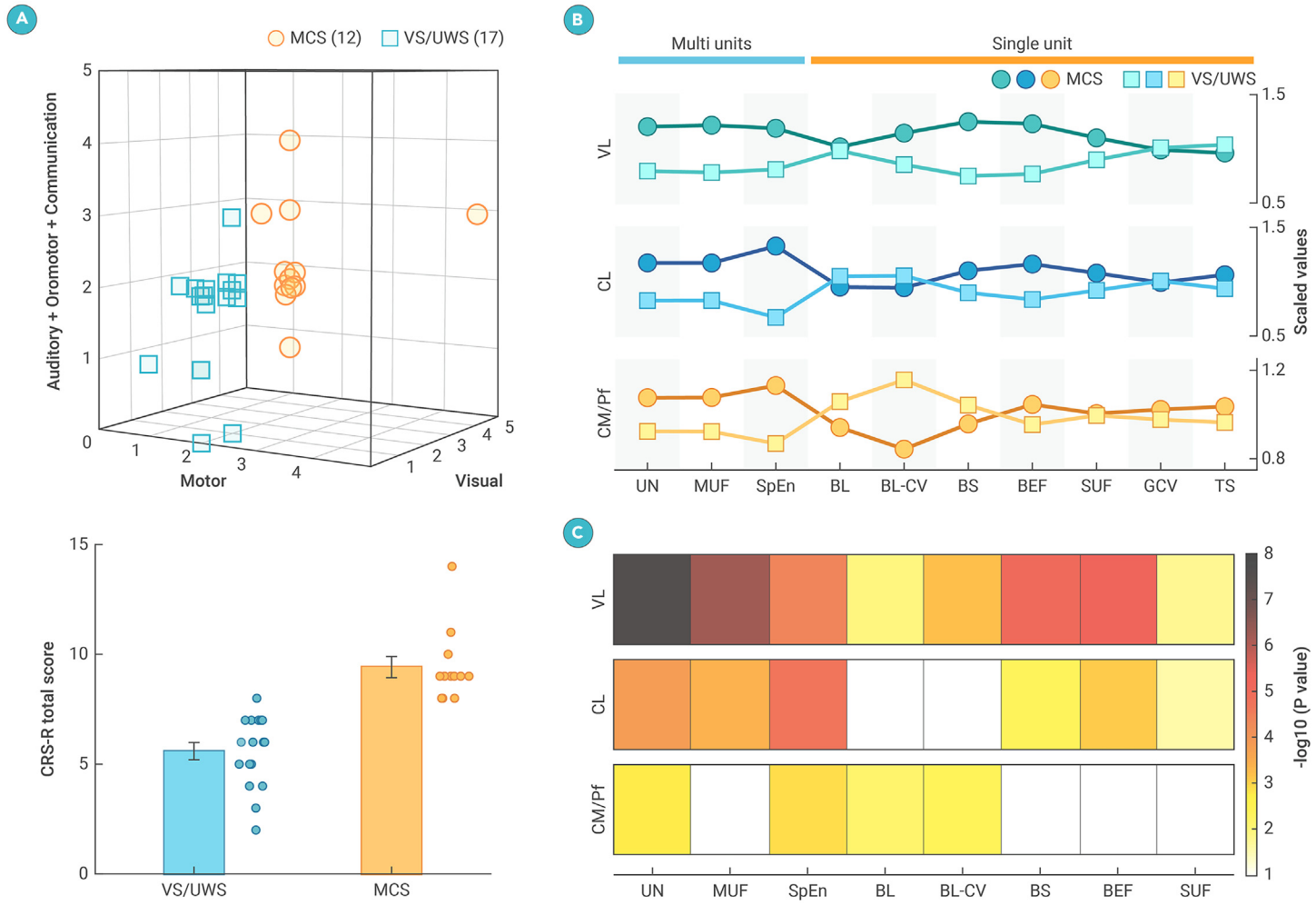

Figure 2. Comparisons of neuronal signatures of thalamic neurons between MCS and VS/UWS patients (A) Top: diagnostic classification of 29 patients into MCS and VS/UWS regarding the classic criteria.[31] Bottom: CRS-R total score of VS/UWS and MCS patients. Data are represented as the mean ± SEM; each dot represents an individual patient. (B) The neuronal signatures in three thalamic nuclei are associated with DoC patients' consciousness states. The scaled values of neuronal signatures were standardized by dividing the responses of each consciousness state by the mean responses across patients. (C) MCS and VS/UWS have different neuronal signatures of the thalamic nuclei, according to Mann-Whitney-Wilcoxon tests. The color map illustrates *p* values. UN, unit number; MUF, multiunit frequency; SpEn, sample entropy; BL, burst length; BL-CV, BL coefficient of variation; BS, burst spike; BEF, burst event frequency; SUF, single-unit frequency; GCV, geometric coefficient of variation of interspike intervals; TS, tonic spike.

(https://www.fieldtriptoolbox.org/).[44] The burst mode was defined by clusters of at least two spikes with interspike intervals shorter than 8 ms (Figure 1F). We calculated firing rates of burst spikes and tonic spikes based on whether the spikes were in burst mode or not. The BEF (burst events per second), BL (spikes per burst),[45] and BL-CV were also calculated. In addition, we established burst events by considering with interspike interval that were less than 5 and 10 ms and yielded comparable results.

SpEn

SpEn was applied to assess the regularity and complexity of time series. It is theoretically similar to approximate entropy but offers greater precision.[46] A low value of SpEn typically indicates a high degree of regularity.[47,48] Here, we utilized SpEn to estimate the irregularity of multiunit activities. Spike trains of multiunits were convolved with a Gaussian kernel having a standard deviation of 25 ms (FieldTrip function ft_spikedensity), in order to obtain continuous signals, and then downsampled to 125 Hz.[47] To calculate the SpEn, a time series of finite length N, $x(i), 1 \le i \le N$, was first embedded with a dimension of m:

$$X_m(i) = \{x(i), x(i+1), x(i+2), x(i+m)\}, i = 1, 2, \ldots, N - m.$$

Then, the probability that $X_m(j)$ is within distance r of $X_m(i)$ was defined as follows:

$$C_i^m(r) = (N - m)^{-1} \sum_{j=1}^{N-m} \Theta(d[X_m(i), X_m(j)] - r),$$

where Θ is the Heaviside function and d is the Chebyshev distance between $X_m(i)$ and $X_m(j)$. The embedding dimension m was set as 3 and distance criterion r was set as 0.2 SD of continuous signals of multiunits.[47]

Finally, the SpEn was defined as:

$$\mathrm{SpEn} = \log\left((N - m)^{-1} \sum_{i=1}^{N-m} C_i^m(r)\right) - \log\left((N - m)^{-1} \sum_{i=1}^{N-m} C_i^{m+1}(r)\right).$$

The measure was implemented by the MATLAB function SpEn (files owned by Kijoon Lee; https://ww2.mathworks.cn/matlabcentral/fileexchange/35784-sample-entropy).

GCV

In order to evaluate the variability in spiking time of each single neuron, we used the following formula to quantify the GCV[49] of interspike intervals below 40 ms:

$$\mathrm{GCV} = \sqrt{e^{S^2} - 1},$$

where S is the standard deviation of interspike intervals. GCV is high when spikes are more sparsely distributed; it is low when spikes are clustered as burst events with regular interspike intervals.

Partial least-squares regression analysis and neuronal index definition

Partial least-squares regression was performed to predict consciousness levels based on patients' CRS-R_{T0} scores and neuronal signatures (independent variables). Only those signatures (four signatures in the CM/Pf, six signatures in the CL, and eight signatures in the VL) that passed the statistical test between MCS and VS/UWS groups were applied in the partial least-squares regression analyses (Figure 2C, MATLAB function plsregress). The partial least-squares model returned the regression coefficient of each neuronal signature and

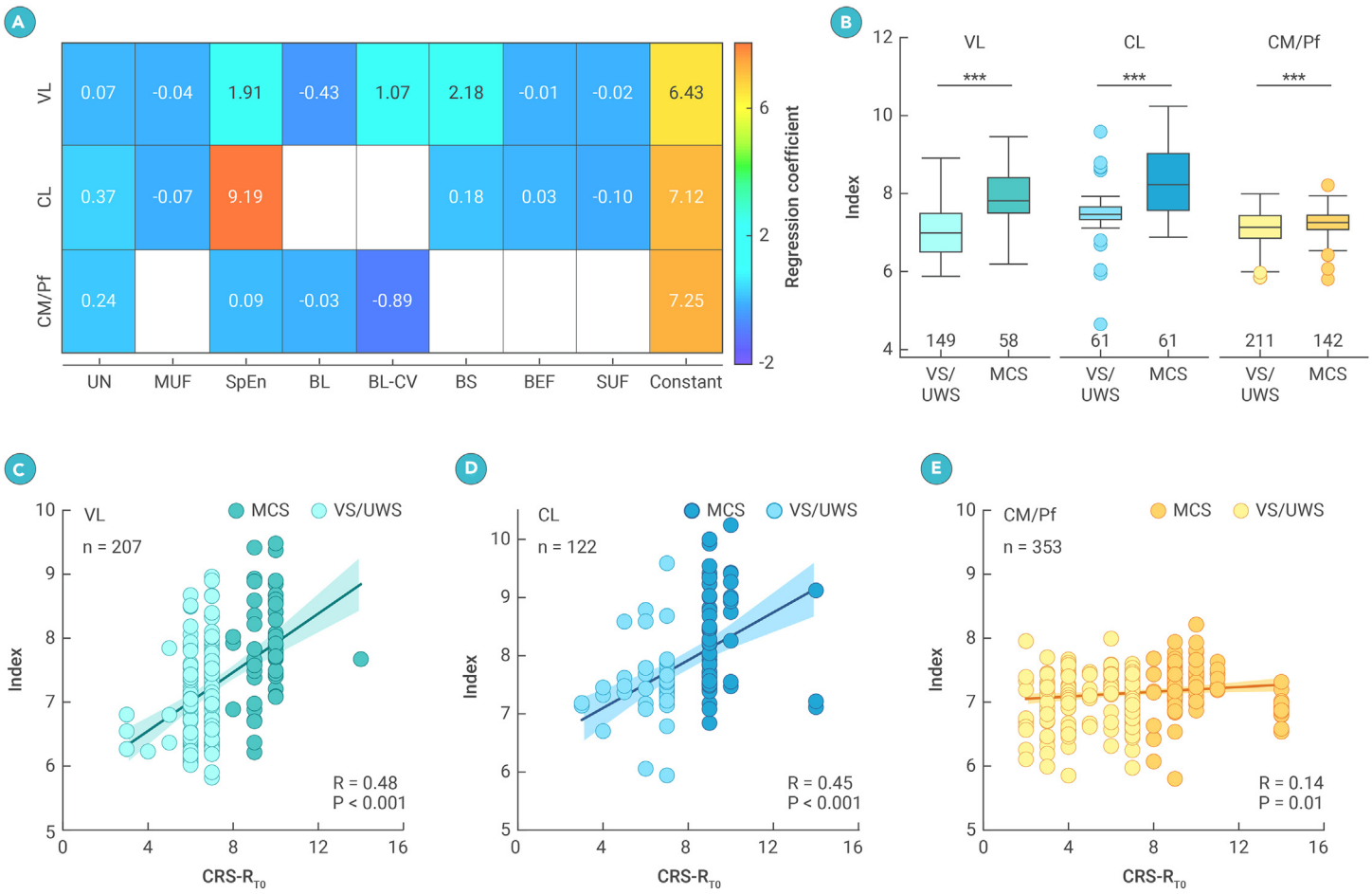

Figure 3. Neuronal index of thalamic neurons indicates DoC patients' consciousness levels (A) The neuronal index was determined based on the obtained partial least-squares regression coefficients. The matrix represents the values of the constant and regression coefficients for three thalamic nuclei. (B) Comparisons of neuronal indices of three thalamic nuclei between MCS and VS/UWS (***$p < 0.001$, Mann-Whitney-Wilcoxon test). The number at the bottom presents the number of recording sites. The boxplot is centered on the median, with boxes representing the 25th and 75th percentiles. Whiskers extend to 1.5 times the interquartile range above the 75th percentile and 1.5 times the interquartile range below the 25th percentile. Points beyond the whiskers are considered outliers. (C–E) Positive correlations were observed between neuronal indices of individual recording sites in three thalamic nuclei and CRS-R$_{T0}$ total scores (C, VL; D, CL; and E, CM/Pf). Black lines represent the linear regression, while shaded areas are the 95% confidence interval of fitting.

the intercept term (Figure 3A). Then, the neuronal index was defined using the following formula:

$$\text{Neuronal Index} = \beta_0 + \sum_{i=1}^{n} \beta_i * S_i,$$

where β_0 is the intercept term, β_i is the regression coefficient of the ith neuronal signature S, n = 8 in the VL, n = 6 in the CL, and n = 4 in the CM/Pf.

Resting-state image preprocessing and effective connectivity analyses

In this study, 18 of 29 patients were accessible for rs-fMRI analysis. fMRI preprocessing and connectivity analyses were carried out as described in previous research.[33] For the analysis of resting-state fMRI images, SPM12 (https://www.fil.ion.ucl.ac.uk/spm/software/spm12/) and freely accessible programs (https://github.com/elifesciences-publications/pDOC) were utilized. The preprocessing steps comprised the elimination of the initial five volumes, slice timing, head motion correction, spatial smoothing with a 6-mm Gaussian kernel, nuisance signal regression, and temporal band-pass filtering (0.01–0.08 Hz). During the nuisance signal regression, linear regression was utilized to eliminate the impact of head motion (12 motion parameters, including roll, pitch, yaw, translation in three dimensions, and their first derivatives), whole-brain signals, and linear trends. To minimize the effects of motion artifact on functional connectivity analysis, framewise displacement of head movement was evaluated, and volumes with large movements also were removed. This is the sum of the absolute values of the translational and rotational realignment estimates' derivatives (after converting the rotational estimates to displacement at 50 mm radius).[50] Volumes with framewise displacement greater than 1.5 mm were discarded, and patients with fewer than 50 remaining volumes were excluded from further analysis. According to these criteria, one (no. 08) of 18 patients with rs-fMRI was discarded. The subsequent effective connectivity (EC) analyses were conducted using the rs-fMRI data from the remaining 17 patients.

Next, we utilized the Dynamic Causal Modeling (DCM) module of SPM12 to examine the EC between thalamic nuclei (CM/Pf and CL) and cortical regions in six brain networks (the default mode, executive control, salience, sensorimotor, auditory, and visual networks, Figures S3A–S3F) as well as between thalamic nuclei and the striatum (Figure S3G). The default mode network includes the anterior medial prefrontal cortex (aMPFC), posterior cingulate cortex/precuneus (PCC), and lateral parietal cortex (LatP). The executive control network consists of the dorsal medial prefrontal cortex (DMPFC), the anterior prefrontal cortex (PFC), the superior parietal cortex (SPC), and the dorsal lateral prefrontal cortex (DLPFC). The orbital frontoinsula (aIns) and the dorsal anterior cingulate cortex (dACC) comprise the salience network. The sensorimotor network includes primary motor cortex (M1) and supplementary motor area (SMA). The primary auditory cortex (A1) and the middle cingulate cortex (MCC) constitute the auditory network. The primary visual cortex (V1) and the associative visual cortex (V4) constitute the vision network. The regions of interest (ROIs) of CM/Pf and CL were established by the Krauth/Morel atlas.[42] The ROIs of cortical regions within six brain networks were identified by the methods developed by Song et al.[33] The ROIs of the striatum were established by the atlas of the basal ganglia (ATAG).[51] The combination of voxels from both hemispheres produced the thalamic ROI and 14 cortical ROIs. The first principal component of the time series from each ROI was computed by SPM12 and saved as the volume of interest for that ROI. These extracted volume of interests were then used in subsequent DCM analysis.

Each thalamocortical DCM model featured CM/Pf or CL and brain regions in a particular network. The EC includes the reciprocal connections between these brain regions, and their self-connections within each region. Given the efficacy of the spectral DCM (sDCM) approach for analyzing rs-fMRI data,[52] these models were estimated for each patient using the sDCM method.[53] The estimated model parameters were averaged across patients using Bayesian fixed-effect averaging (spm_dcm_average). Group-level analyses were performed using the parametric empirical Bayes (PEB) method (spm_dcm_peb and

spm_dcm_peb_bmc).[54] The effects of neuronal signatures and GOS were evaluated by specifying them as the covariates of the second-level design matrix. The design matrix consisted of two columns of covariates: the first column was a vector of ones (to model the commonality effect across patients, i.e., the constant or group mean) and the second column represented the between-subject influences of neuronal signatures or GOS (mean centered). Before being specified as a covariate, a given neuronal signature was averaged across CM/Pf neurons for each patient, and then the mean values of that signature were *Z* scored across patients. To focus on the parameters with stronger evidence, we applied a threshold to the Bayesian model average in PEB, selecting only those having a 99% posterior probability of being present vs. absent (thresholding based on free energy, Figures 6E, 6F, S4A, S4B, S5G, S5I, and S5J).

Structural connectome

We analyzed the structural connectome between the thalamic nuclei and the cortical areas, as well as the striatum (Figures S3H and S3I), using diffusion MRI data of DoC patients, conducted by DSI-Studio (https://dsi-studio.labsolver.org/). After preprocessing (motion correction and removing eddy current distortion), the 1.25-mm isotropic resolution spin distribution function of each patient was reconstructed to MNI space. This reconstruction was achieved using the Q-space diffeomorphic reconstruction method,[55] with a diffusion sampling length ratio of 1.25.

A deterministic fiber tracking algorithm was utilized to achieve whole brain tracking with the following parameters: angular threshold 0, step size 0, minimum length 30 mm, maximum length 300 mm, and number of tracts 1,000,000. The ROIs of the cortical areas were defined using the HCP-MMP atlas[56] built-in DSI-Studio, the ROIs of the striatum were defined using ATAG,[51] and the ROIs of the thalamic nuclei were defined using the Krauth/Morel atlas.[42] The connectivity matrix was calculated by considering the number of tracts that pass through paired ROIs. For each DoC patient, a threshold of 0.001[57] (the ratio to the maximum connecting tracks in the connectivity matrix) was used to filter out the connectivity matrix. Connectivity matrices of individuals were averaged to obtain the group-level matrix, which was also filtered out using a threshold of 0.001.

Feature selection and logistic regression analyses

Feature selection was conducted using the algorithm of f_classif implanted in the Python library of Scikit-learn.[58] It computes the analysis of variance (ANOVA) F value to select the most distinguishing features between consciousness recovery and non-recovery groups. Two independent classification analyses were separately performed on 10 neuronal signatures and 32 brain connections (30 connections between thalamic nuclei and cortical regions and 2 connections between thalamic nuclei and the striatum). Binary classifications were performed using penalized logistic regression through the algorithm of LogisticRegression of Scikit-learn.[58] Briefly, the label y_i of data point i takes values in the set [0, 1] (0 for consciousness non-recovery and 1 for recovery), and the probability of positive class was predicted as:

$$p = \frac{1}{1+e^{-(\beta_0+\beta_i X_i)}},$$

where β_0 is the intercept of the logistic regression model, β_i is the slope coefficients of the model, and X_i are features. To optimize model parameters, the L2 regularization term $r(\beta)$ was combined to minimize the cost function:

$$\min C \sum_{i=1}^{n} (-y_i \log p - (1-y_i)\log(1-p)) + r(\beta).$$

The logistic regression classification was cross-validated using the k-folds method (5 folds for neuronal signatures and 4 folds for EC) and repeated 1,000 times to establish stability in feature importance histograms (Figures 4G, 4H, 6E, and S5G) and AUC scores (Figure 6G). The shuffling analysis was conducted by randomly permuting class labels 1,000 times, and the output of the logistic classifier was compared with results of the shuffled data.

Statistical analysis

The neuronal signatures and neuronal indices of MCS and VS/UWS patients (Figures 2C and 3B), as well as neuronal signatures between the recovery and the non-recovery groups (Figures 4A–4F, 4H, 5C, 5D, and S5A–S5E) were compared utilizing a Mann-Whitney-Wilcoxon test. The frequency of single-unit and multiunit activity in the CM/Pf, the CL, and the VL were compared using a one-way ANOVA, followed by a *post hoc* Tukey-Kramer test for pairwise comparisons between thalamic nuclei (Figures S1D and S1E). Statistical analysis was conducted to determine the comparisons, using a significance level of 0.05. Pearson's correlation coefficient was used to measure the correlation between neuronal index and CRS-R_{T0} and between neuronal signatures and GOS scores (Figures 3C–3E, 6C, 6D, S2A, S2B, and S5H).

RESULTS

Neuronal signatures of thalamic neurons indicate DoC patients' consciousness levels

We first describe the thalamic microelectrode recordings. All recorded single units were sorted offline and remapped according to reconstructed DBS lead trajectories (Figure 1A, bilateral leads from patient no. 26 as an example; Figure S1C, leads for all 29 patients). As depicted in Figure 1B, the lead has traversed the VL and the CL before landing its C0 contact into the CM/Pf of the thalamus. A total of 960 thalamic neurons were recorded from 682 sites across three thalamic nuclei in 29 patients (Figure 1C), exhibiting both tonic and burst firing modes (Figures 1D–1F). To comprehensively characterize the spiking activity of these neurons, we analyzed 10 spike-based neuronal signatures at both the single-unit and the multiunit levels (see materials and methods for details).

Next, we evaluated the relationship between thalamic neuronal activities and levels of consciousness. Patients were categorized according to their preoperative consciousness states, VS/UWS (17 patients) and MCS (12 patients) (Figure 2A), employing the JFK CRS-R[31] (see Table S1 for details). We then independently compared 10 neuronal signatures in the thalamic nuclei, VL, CL, and CM/Pf (Figure 2B) and identified differences in these signatures between the two consciousness states (Figure 2C). Patients with VS/UWS who had lower levels of consciousness exhibited less active thalamic neurons, characterized by longer and more variable burst discharges in the CM/Pf, as well as reduced burst firing activities in the CL and VL (Figures 2B and 2C), compared to those in MCS. These signatures in thalamic nuclei, particularly burst discharges of single neurons, effectively distinguished VS/UWS from MCS.

To synthesize these signatures, we established a neuronal index based on those that significantly differed between VS/UWS and MCS patients, utilizing a partial least-squares regression model (see materials and methods for details; Figure 3A). Neuronal indices from three thalamic nuclei differed between VS/UWS and MCS patients (Figure 3B, $p < 0.001$, Mann-Whitney-Wilcoxon test) and exhibited consistent upward trends in relation to patients' total CRS-R scores (CRS-R_{T0}, Figures 3C–3E), with lower scores corresponding to smaller indices and progressively higher scores associated with larger indices. The thalamic neuronal index not only differentiates MCS from VS/UWS but also correlates with consciousness levels. Clinical factors, such as the interval injury to DBS surgery and the etiology, likely influence neuronal activity and contribute to shaping the neuronal index. It is noteworthy that the neuronal indices of thalamic nuclei consistently grade patients' consciousness levels, with linear regression analysis confirming this relationship while controlling for the effects of interval injury and etiology (Figures S2A and S2B).

Thalamic spiking serves as an indicator of arousal regulations following DBS in DoC patients

Seven days postsurgery, thalamic DBS was administered via the C0 contact of electrodes centered in the CM/Pf. As the direct treatment site, we examined whether neuronal signatures of the CM/Pf signal outcomes following DBS. We assessed patients' recovery outcomes within 12 months using the GOS and monitored their follow-up consciousness states by CRS-R score (CRS-R_{T12}) (Figure S1). Ten patients recovered consciousness (recovered, GOS $\geq$ 3). Their follow-up total CRS-R scores increased from 9 ± 3 (mean ± SD, CRS-R_{T0}) to 18 ± 4 (CRS-R_{T12}). The remaining 19 patients did not recover consciousness (non-recovered, GOS $\leq$ 2); their total CRS-R scores evolved from 6 ± 2 (CRS-R_{T0}) to 7 ± 2 (CRS-R_{T12}). Neuronal activities of the CM/Pf in the recovered patients showed higher tonic firing rates and variations of interspike intervals in single units, as well as more active neurons with higher spiking activities in multiunit analyses (Figures 4A–4F, Mann-Whitney-Wilcoxon test, tonic spikes, $p = 1.55 \times 10^{-4}$; GCV, $p = 8.63 \times 10^{-5}$; single-unit frequency, $p = 5.56 \times 10^{-3}$; multiunit frequency, $p = 9.18 \times 10^{-4}$; SpEn, $p = 1.53 \times 10^{-2}$; unit number, $p = 6.47 \times 10^{-3}$).

We identified how these six neuronal signatures in the CM/Pf contribute to discriminating the recovered group from the non-recovered group using a cross-validated supervised machine learning model (see materials and methods for details). The model indicated that five of them (excepting single-unit frequency) can sensitively signal recovery outcomes (GOS $\geq$ 3 vs. GOS $\leq$ 2) in 29 patients following DBS (defined by F score, ANOVA, Figure 4G). Prior to

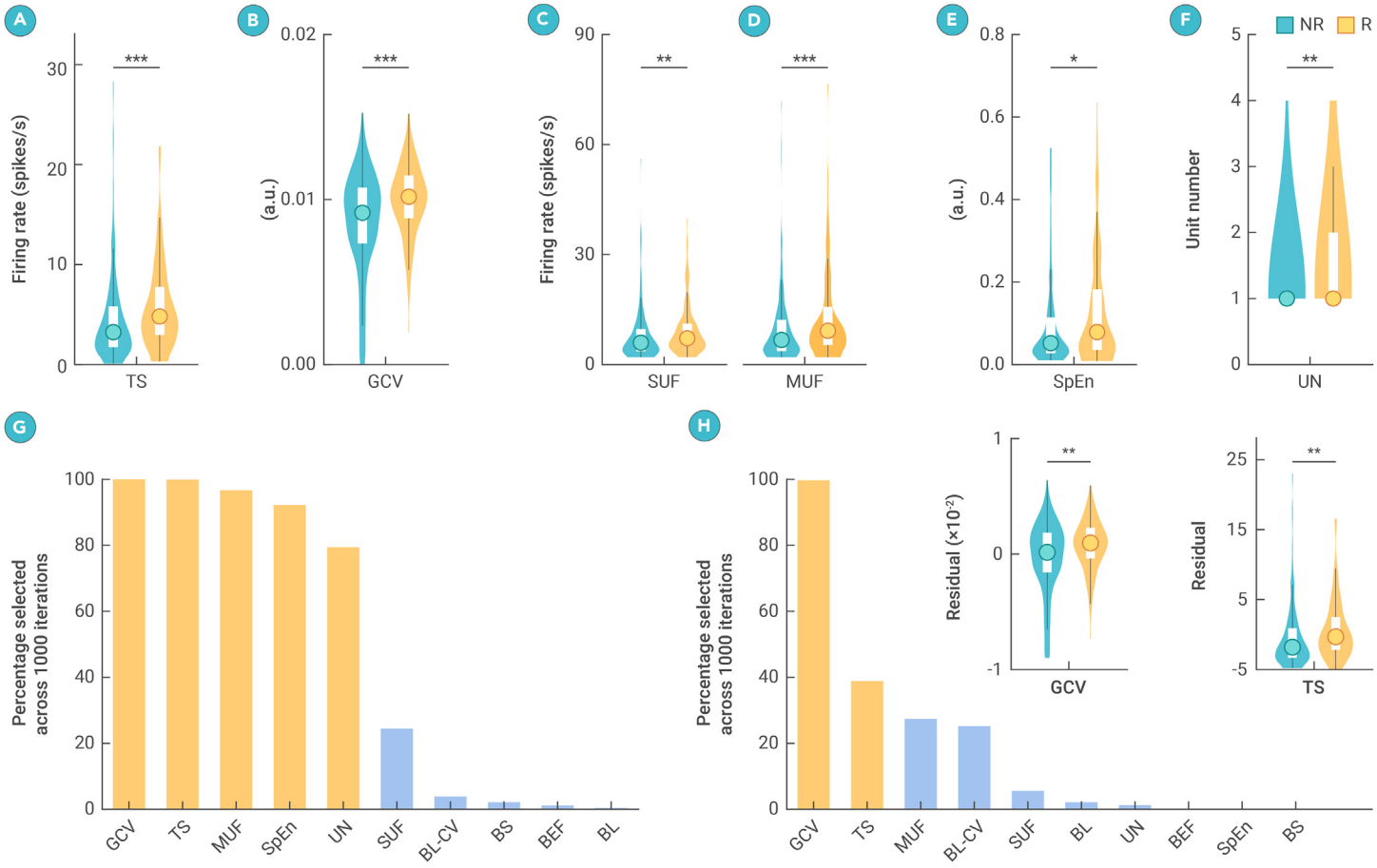

Figure 4. Thalamic neuronal signatures of the CM/Pf indicate arousal regulation following DBS in DoC patients (A–F) Comparison of tonic firing rates (TS), geometric coefficient of variation (GCV), single-unit frequency (SUF), multiunit frequency (MUF), sample entropy (SpEn), and neuronal unit number (UN) in the CM/Pf between recovered (119 recording sites from 10 patients) and non-recovered (234 recording sites from 19 patients) groups. *$p < 0.05$, **$p < 0.01$, and ***$p < 0.001$, Mann-Whitney-Wilcoxon test. (G) Five top neuronal signatures of the CM/Pf were able to differentiate between recovered and non-recovered (defined by F values, ANOVA) by using a cross-validated supervised machine learning model. (H) Elimination of the impact of patients' preoperative consciousness states on neuronal signatures by a linear regression. GCV and TS of the CM/Pf consistently and effectively differentiate between recovered and non-recovered groups. The violin plots are centered on the median, with boxes indicating the 25th and 75th percentiles. Whiskers extend 1.5 times the interquartile range above the 75th percentile and 1.5 times the interquartile range below the 25th percentile, with points beyond the whiskers classified as outliers. R, recovered; NR, non-recovered.

DBS, the average consciousness level in the recovered group (8 patients in MCS and 2 patients in VS/UWS) was notably higher than that of the non-recovered group (4 patients in MCS and 15 patients in VS/UWS), potentially leading to varied recovery outcomes. Thus, these five thalamic signatures identified here might primarily serve as indicators to represent consciousness levels, rather than playing roles in arousal regulation or predicting outcomes. We ruled out this possibility by employing a linear regression analysis to control the effect of recovered and non-recovered patients' preoperative consciousness state. The residuals from the regression analysis revealed that single-unit spiking activity could indicate recovery outcomes following DBS. Key indicators included the firing rates of tonic spikes (Figure 4H, Mann-Whitney-Wilcoxon test, $p = 1.42 \times 10^{-3}$) and the GCVs of interspike intervals ($p = 3.27 \times 10^{-3}$).

To evaluate whether the neurons analyzed here were directly modulated by DBS, we simulated the VTA around the C0 contact in the three thalamic nuclei. We calculated activation ratios of each nucleus by dividing the VTA by the total volume of that nucleus (Figure 5A). The results showed that 24.0% of the CM/Pf, 0.7% of the CL, and 0.3% of the VL were activated by DBS across 29 patients (Figure 5B). The existence of VTAs in the CL and VL raised the possibility that DBS-activated neurons in these nuclei might also contribute to recovery following DBS. However, when comparing recovery outcomes between patients with activation ratios greater than 1% or 2% in the CL and VL and those with lower ratios, the data failed to support this possibility. Neither GOS scores (1%, CL, $p = 0.54$, and VL, $p = 0.82$; 2%, CL, $p = 0.83$) nor changes in total CRS-R scores following DBS (1%, CL, $p = 0.37$, and VL, $p = 1.00$; 2%, CL, $p = 0.74$) were able to differentiate between the two groups. Thus, we focused on the CM/Pf's neurons located in the VTA regions of the recovered and non-recovered groups. The data revealed higher single-unit tonic firing (Figure 5C) as well as greater variation of interspike intervals (Figure 5D) in the recovered group. Note that these two neuronal signatures in the CM/Pf, as prospective prognostic indicators, did not differentiate between consciousness levels (Figure 2C). These findings suggest that neuronal mechanisms responsible for altering levels of consciousness may be distinct from those involved in representing different states of consciousness.

Thalamic neuronal signatures linked with thalamocortical connections predict recovery outcomes

The thalamus assumes the responsibility of regulating arousal through its connections within brain networks, including the cerebral cortex and striatum. We examined a subgroup of 17 patients who obtained qualified rs-fMRI data and conducted three independent additional analyses to explore the relationships between thalamic signatures, brain connections, and DBS outcomes (Figure 6A).

First, we analyzed the relationship between EC and recovery outcomes. Using DCM (Figures 6B and S3A–S3F), we investigated 30 connections between the CM/Pf and 15 cortical areas across six functional brain networks, namely the default mode network, executive control network, salience network, sensorimotor network, auditory network, and visual network, along with 2 connections between the CM/Pf and the striatum (Figure S3G). Next, we reexamined the correlation between neuronal signatures in the CM/Pf and recovery outcomes in these 17 patients, confirming that both tonic spikes and the GCVs in interspike intervals in the CM/Pf were significantly associated with GOS scores (Figures 6C and 6D). Finally, we utilized PEB analysis to investigate how CM/Pf neuronal signatures influence brain connectivity (Figure 6E).

Through these analyses, we identified six ECs forming "logic loops" (Figures S4A and S4B), which establish closed-loop logical linkages among ECs, neuronal signatures, and GOS scores through positive or negative

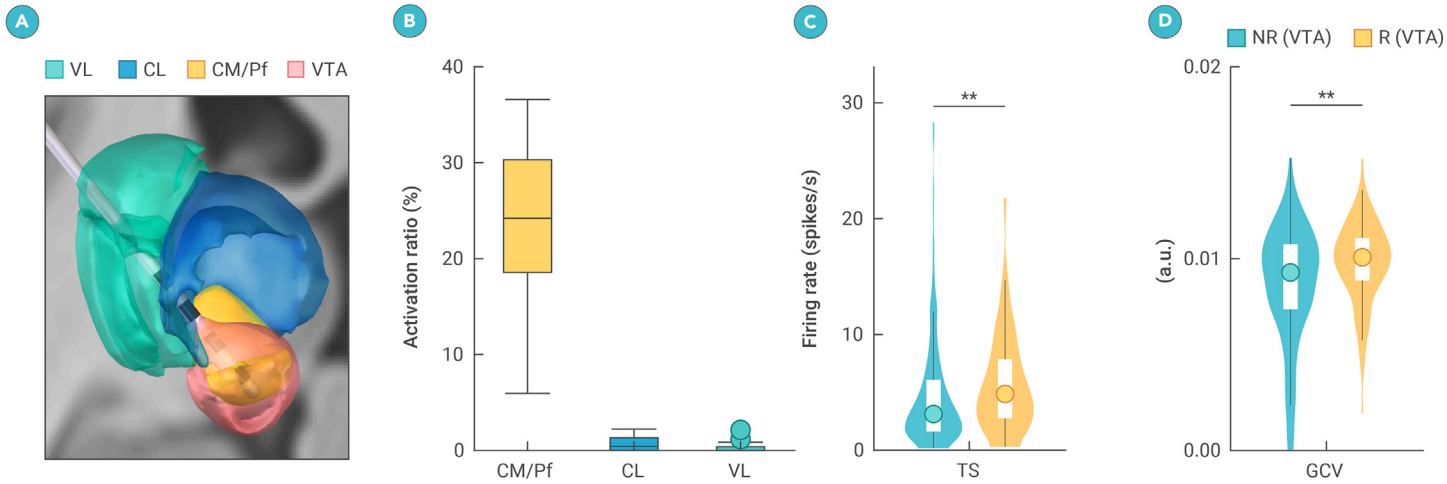

Figure 5. Characterization of the DBS VTA and its neuronal signatures (A) Estimation of the DBS VTA (red area) through the C0 contact in the example DoC patient (shown in Figure 1B). (B) Activation ratios represent the proportion of the VTA within each nucleus across patients relative to the total volume of that nucleus. (C and D) Comparisons of TS (C) and GCV (D) of recording sites located within the VTA area of the CM/Pf between the recovered and the non-recovered groups. The violin and boxplots are centered on the median, with boxes indicating the 25th and 75th percentiles. Whiskers extend 1.5 times the interquartile range above the 75th percentile and 1.5 times the interquartile range below the 25th percentile, with points beyond the whiskers classified as outliers. VTA, volume of tissue activated.

correlations. These ECs included key areas such as the aMPFC, SPC, dACC, A1, and PFC. Notably, most of them are integral to thalamoparietal and thalamofrontal networks involved in consciousness and wakefulness. In contrast, no statistically significant differences were observed in the connections between the CM/Pf and the striatum between recovered and non-recovered groups (Mann-Whitney-Wilcoxon test; $EC_{CM/Pf\text{-}Striatum}$, $p = 0.19$; $EC_{Striatum\text{-}CM/Pf}$, $p = 0.28$). The extensive thalamostriatal connections in patients might have potentially prevented its accuracy of recovery prediction.

To further verify the impact of these brain connections on recovery outcomes, we utilized a cross-validated supervised machine learning model with feature selection. The analysis identified the most pivotal connection distinguishing between recovered and non-recovered patients (Figure 6E): the EC from CM/Pf to aMPFC in the default mode network ($EC_{CM/Pf\text{-}aMPFC}$). Within the identified logic loops (Figure 6F), higher tonic firing rates and greater variability of interspike intervals in the CM/Pf correlated with better recovery outcomes, as reflected by higher GOS scores and enhanced $EC_{CM/Pf\text{-}aMPFC}$. Logistic regression classification further confirmed that the top selected factors, including tonic spike firing rates, GCV, and $EC_{CM/Pf\text{-}aMPFC}$, effectively discriminated recovered patients from non-recovered ones, achieving an area under the curve (AUC) of 0.84 (Figure 6G). These findings indicate that neuronal signatures in the CM/Pf (tonic spikes and GCV) could influence recovery by modulating $EC_{CM/Pf\text{-}aMPFC}$. Consequently, the CM/Pf emerges as a critical target for DBS, potentially serving as a key node in regulating arousal within neuronal networks.

DISCUSSION

In this study, we investigated cellular events that occur in the thalamic nuclei of patients diagnosed with VS/UWS and MCS, at both single-neuron and multiple-neuron levels. Notably, the firing modes of thalamic neurons emerged as a critical feature. Our findings highlight that thalamic firing activity, especially the burst discharge of single neurons, serves as a critical marker for the representation of consciousness in DoC patients. Specifically, patients in a VS/UWS who experienced lower levels of consciousness demonstrated prolonged and more variable burst discharges in the CM/Pf compared to those in MCS, who displayed higher levels of consciousness. Previous research has linked shorter BL to stronger γ-aminobutyric acid-ergic (GABAergic) inhibition in the system, with GABA application in the striate cortex shortening BL, and $GABA_A$ receptor blocker via bicuculline prolonging it.[45] In DoC patients with traumatic brain injury, widespread reductions in $GABA_A$ receptor availability, predominantly in the frontal lobes, striatum, and thalamus,[59] may account for the observed longer BL. These findings suggest that similar neuronal mechanisms underlie burst activity in both cortical and subcortical regions, potentially reflecting consciousness-related processes.

Intriguingly, single-unit signatures in the CM/Pf associated with recovery outcomes, particularly tonic discharges, are distinct from those grading consciousness levels, such as burst firing. Previous studies have demonstrated that burst and tonic discharges serve distinct roles in brain functions. For instance, rapid switching between these firing modes in mice can govern the transition of sleep-wake states[8] or the generalization of epilepsy[60] in a bidirectional manner. Burst firing can trigger slow-wave-like activity or initiate absence epilepsy, whereas tonic activation promotes sleep recovery or terminates the epileptic symptoms. Our results demonstrated that central thalamus is a key region for both the representation and the alteration of consciousness but via distinct neuronal mechanisms. Burst and tonic discharge of thalamic neurons appear to play crucial, yet differentiated, roles in these processes.

The thalamocortical pathway is central to recovery in DoC. Our findings suggest that EC between the CM/Pf and the aMPFC plays a crucial role in promoting recovery in DoC. Increasing evidence demonstrates that DoC is characterized by severe disruptions in intrinsic brain activity, diminished default mode network connectivity, and altered cross-network dynamics.[61–69] As a key node within the default mode network, the aMPFC exhibits functional connectivity with the dorsomedial prefrontal cortex that correlates with patients' CRS-R scores, positioning it as a potential predictor of recovery outcomes.[33] Furthermore, the modulation of aMPFC connectivity across sleep states[70] and its attenuation under sedation[71] further suggest its integral role in consciousness. The anterior forebrain mesocircuit model underscores the crucial role of the thalamus in consciousness alterations,[12] facilitated by connections to the frontal and parietal cortices (Schiff,[13] Ilyas et al.,[72] Sadikot and Rymar,[73] Benarroch,[74] Harris et al.,[75] Arnts et al.,[76] Mandelbaum et al.[77]; our data in Figures S3H and S3I). Intriguingly, we observed that tonic firing in the CM/Pf selectively influenced the unidirectional connection from the CM/Pf to the aMPFC, without affecting the reverse direction (Figure S4). Given the observed effect on the unidirectional connection, higher tonic firing in the thalamus may be amenable to DBS interventions aimed at improving recovery, particularly through modulating of the $EC_{CM/Pf\text{-}aMPFC}$ (Figure 6). These findings provide important insights into neuronal mechanisms underlying thalamic DBS in regulating arousal states.

Previous research in anesthetized animals demonstrated that DBS targeting the intralaminar thalamus, including both the CM/Pf and the CL, can effectively modulate cortical networks and lead to arousal-related functional responses. CM/Pf-DBS has been shown to influence a broad range of brain regions, including the prefrontal, parietal, cingulate, temporal, and occipital cortices, as well as the striatum.[26,27] It restores the collapsed principle gradient of functional connectivity and mitigates reduced network hierarchical integration induced by anesthesia.[28] These effects may be mediated through connections between the CM/Pf and cortical regions, such as the thalamostriatal-cortical pathway,[72,73] contributing to the restoration of arousal. Meanwhile, CL-DBS could be involved in altering consciousness by enhancing interactions in the frontal eye field and the lateral intraparietal area[10] and regulating arousal.[10,13,78] Therefore, we further evaluated the CL's contribution to DBS effects in these patients. Five neuronal

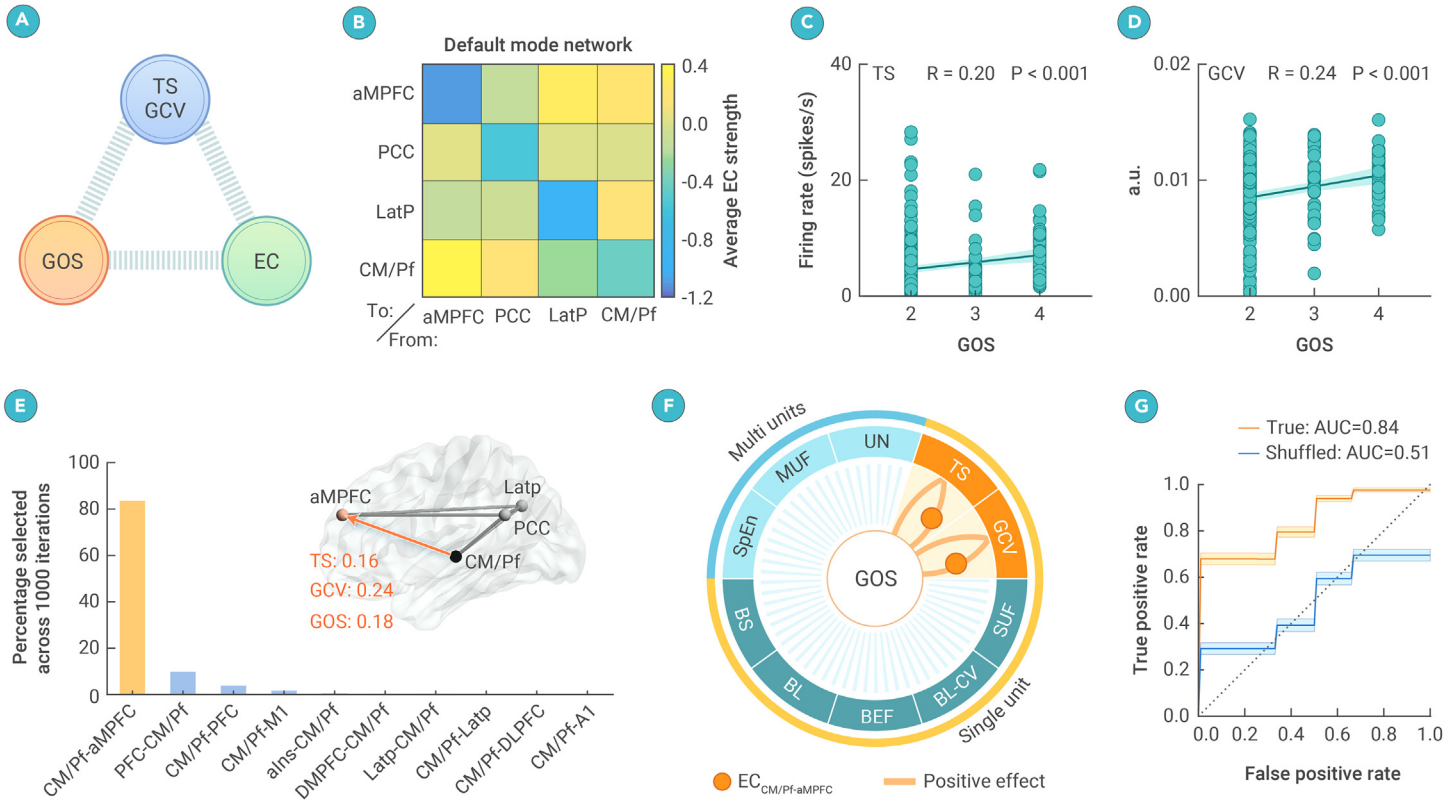

Figure 6. DoC patients' thalamic firing linked with thalamocortical connections to predict outcomes following DBS (A) Schematic diagram of pairwise relationships between neuronal signatures, GOS scores, and effective connectivity. (B) Effective connectivity between the CM/Pf and cortical areas in the default mode network, averaging across 17 patients with qualified rs-fMRI data. (C and D) Correlation between neuronal signatures of 306 recording sites from 17 patients (TS, C, and GCV, D) and their GOS scores, measured by Pearson's correlation coefficient. The solid lines represent linear regression, whereas shaded areas represent 95% confidence intervals. (E) The top connection selected by F values of an ANOVA was able to discriminate the recovered group from the non-recovered group in our dataset. The thalamocortical connection from the CM/Pf to the aMPFC was positively correlated with GOS scores and thalamic neuronal signatures, with related effect sizes given in red font. (F) Summary of relationships between thalamic signatures, ECs, and DBS outcomes in DoC patients. The ring contains 10 neuronal signatures of the CM/Pf. Seven of them were defined from single units (yellow arcs), while the remaining three signatures were estimated from multiple units (blue arcs) of each recording site. Orange spots present the $EC_{CM/Pf\text{-}aMPFC}$. Lines indicate "logic" loops of correlations between neuronal signatures (TS and GCV), the $EC_{CM/Pf\text{-}aMPFC}$, and GOS scores, with peach lines representing positive effects. (G) Receiver operating characteristic curves to predict recovery outcomes based on the top neuronal signatures (TS and GCV) and the top connection ($EC_{CM/Pf\text{-}aMPFC}$) from individual patients, reflecting the mean ± SEM over 1,000 times for the true (orange) and shuffled (blue) models. PCC, posterior cingulate cortex/precuneus; PFC, anterior prefrontal cortex; M1, primary motor cortex; aIns, orbital frontoinsula; DMPFC, dorsal medial prefrontal cortex; LatP, lateral parietal cortex; DLPFC, dorsal lateral prefrontal cortex; A1, primary auditory cortex.

signatures in the CL differed significantly between the recovered and the non-recovered groups (Figures S5A–S5E, Mann-Whitney-Wilcoxon test, $p < 0.05$). Utilizing linear regression analysis to control patients' preoperative consciousness states, we verified that the GCV in the CL, as well as the $EC_{CL\text{-}aIns}$ and $EC_{CL\text{-}aMPFC}$, consistently discriminated recovered individuals from the non-recovered patients in our dataset (Figures S5F and S5G). Nevertheless, the GCV of CL did not significantly correlate with either brain connections or GOS scores (Figure S5H), failing to support the logic loops (Figures S5I and S5J). Possible reasons could include the presence of a limited number of recording sites in the CL along the microelectrode punctures and a scarcity of electrically activated volumes in the CL (Figure 5B) by DBS in these patients.

The question of how the thalamus modulates consciousness is answered in the most detail for the representation of consciousness and effects on arousal regulation using DBS in a group of 29 patients with DoC. We anticipate that these findings may pave the way for the development of targeted interventions and prognostication strategies for affected individuals. Stronger tonic firing in the thalamus, as identified here, may serve as a key factor when optimizing DBS parameters for therapeutic purposes. Looking beyond DoC, it is highly likely that the thalamic mechanisms underlying consciousness will apply to other brain diseases. Disorders such as epilepsy and Parkinson's disease may also be characterized by thalamic spiking activity and thalamocortical connectivity, offering promising avenues for DBS-based treatments and outcome predictions in these conditions.

DATA AND CODE AVAILABILITY

Datasets supporting the findings of this study are available from the corresponding authors on reasonable request. A spike sorting toolbox Wave_clus was used to identify neuronal spikes (https://github.com/csn-le/wave_clus). SPM12 (https://www.fil.ion.ucl.ac.uk/spm/software/spm12/) and freely accessible programs (https://github.com/elifesciences-publications/pDOC) were used to analyze rs-fMRI data. Trajectories of DBS leads were reconstructed using Lead-DBS software (https://www.lead-dbs.org/). The analyses of ISI and spike train convolution of multiunits were performed by Fieldtrip software (https://www.fieldtriptoolbox.org/). PLS regression was achieved using the MATLAB function plsregress. The computation of SpEn was based on the MATLAB function SpEn (https://ww2.mathworks.cn/matlabcentral/fileexchange/35784-sample-entropy, files owned by Kijoon Lee). Feature selection and cross-validated logistic regression were conducted using Scikit-learn (https://scikit-learn.org). Custom codes used in the study are available from the corresponding authors on request.

REFERENCES

1. Sherman, S.M. (2001). Tonic and burst firing: dual modes of thalamocortical relay. *Trends Neurosci.* **24**:122–126. DOI:https://doi.org/10.1016/s0166-2236(00)01714-8.
2. Swadlow, H.A. and Gusev, A.G. (2001). The impact of 'bursting' thalamic impulses at a neocortical synapse. *Nat. Neurosci.* **4**:402–408. DOI:https://doi.org/10.1038/86054.
3. Borden, P.Y., Wright, N.C., Morrissette, A.E. et al. (2022). Thalamic bursting and the role of timing and synchrony in thalamocortical signaling in the awake mouse. *Neuron* **110**:2836–2853.e8. DOI:https://doi.org/10.1016/j.neuron.2022.06.008.
4. Saalmann, Y.B. and Kastner, S. (2011). Cognitive and perceptual functions of the visual thalamus. *Neuron* **71**:209–223. DOI:https://doi.org/10.1016/j.neuron.2011.06.027.
5. Usrey, W.M. (2002). The role of spike timing for thalamocortical processing. *Curr. Opin. Neurobiol.* **12**:411–417. DOI:https://doi.org/10.1016/S0959-4388(02)00339-2.
6. Sherman, S.M. and Guillery, R.W. (2002). The role of the thalamus in the flow of information to the cortex. *Philos. Trans. R. Soc. Lond. B Biol. Sci.* **357**:1695–1708. DOI:https://doi.org/10.1098/rstb.2002.1161.
7. Krahe, R. and Gabbiani, F. (2004). Burst firing in sensory systems. *Nat. Rev. Neurosci.* **5**:13–23. DOI:https://doi.org/10.1038/nrn1296.

8. Gent, T.C., Bandarabadi, M., Herrera, C.G. et al. (2018). Thalamic dual control of sleep and wakefulness. *Nat. Neurosci.* **21**:974–984. DOI:https://doi.org/10.1038/s41593-018-0164-7.
9. Glenn, L.L. and Steriade, M. (1982). Discharge rate and excitability of cortically projecting intralaminar thalamic neurons during waking and sleep states. *J. Neurosci.* **2**:1387–1404. DOI:https://doi.org/10.1523/JNEUROSCI.02-10-01387.1982.
10. Redinbaugh, M.J., Phillips, J.M., Kambi, N.A. et al. (2020). Thalamus Modulates Consciousness via Layer-Specific Control of Cortex. *Neuron* **106**:66–75. DOI:https://doi.org/10.1016/j.neuron.2020.01.005.
11. Magrassi, L., Zippo, A.G., Azzalin, A. et al. (2018). Single unit activities recorded in the thalamus and the overlying parietal cortex of subjects affected by disorders of consciousness. *PLoS One* **13**:e0205967. DOI:https://doi.org/10.1371/journal.pone.0205967.
12. Edlow, B.L., Claassen, J., Schiff, N.D. et al. (2021). Recovery from disorders of consciousness: mechanisms, prognosis and emerging therapies. *Nat. Rev. Neurol.* **17**:135–156. DOI:https://doi.org/10.1038/s41582-020-00428-x.
13. Schiff, N.D. (2008). Central thalamic contributions to arousal regulation and neurological disorders of consciousness. *Ann. N. Y. Acad. Sci.* **1129**:105–118. DOI:https://doi.org/10.1196/annals.1417.029.
14. Schiff, N.D. (2010). Recovery of consciousness after brain injury: a mesocircuit hypothesis. *Trends Neurosci.* **33**:1–9. DOI:https://doi.org/10.1016/j.tins.2009.11.002.
15. Giacino, J.T., Fins, J.J., Laureys, S. et al. (2014). Disorders of consciousness after acquired brain injury: the state of the science. *Nat. Rev. Neurol.* **10**:99–114. DOI:https://doi.org/10.1038/nrneurol.2013.279.
16. Martin, R.A., Cukiert, A. and Blumenfeld, H. (2021). Short-term changes in cortical physiological arousal measured by electroencephalography during thalamic centromedian deep brain stimulation. *Epilepsia* **62**:2604–2614. DOI:https://doi.org/10.1111/epi.17042.
17. Xu, J., Galardi, M.M., Pok, B. et al. (2020). Thalamic Stimulation Improves Postictal Cortical Arousal and Behavior. *J. Neurosci.* **40**:7343–7354. DOI:https://doi.org/10.1523/JNEUROSCI.1370-20.2020.
18. Monti, M.M., Rosenberg, M., Finoia, P. et al. (2015). Thalamo-frontal connectivity mediates top-down cognitive functions in disorders of consciousness. *Neurology* **84**:167–173. DOI:https://doi.org/10.1212/WNL.0000000000001123.
19. Schiff, N.D., Giacino, J.T., Kalmar, K. et al. (2007). Behavioural improvements with thalamic stimulation after severe traumatic brain injury. *Nature* **448**:600–603. DOI:https://doi.org/10.1038/nature06041.
20. Vanhoecke, J. and Hariz, M. (2017). Deep brain stimulation for disorders of consciousness: Systematic review of cases and ethics. *Brain Stimul.* **10**:1013–1023. DOI:https://doi.org/10.1016/j.brs.2017.08.006.
21. Chudy, D., Deletis, V., Paradžik, V. et al. (2023). Deep brain stimulation in disorders of consciousness: 10 years of a single center experience. *Sci. Rep.* **13**:19491. DOI:https://doi.org/10.1038/s41598-023-46300-y.
22. Yang, Y., He, Q., Dang, Y. et al. (2023). Long-term functional outcomes improved with deep brain stimulation in patients with disorders of consciousness. *Stroke Vasc. Neurol.* **8**:368–378. DOI:https://doi.org/10.1136/svn-2022-001998.
23. Arnts, H., Tewarie, P., van Erp, W.S. et al. (2022). Clinical and neurophysiological effects of central thalamic deep brain stimulation in the minimally conscious state after severe brain injury. *Sci. Rep.* **12**:12932. DOI:https://doi.org/10.1038/s41598-022-16470-2.
24. Arnts, H., Tewarie, P., van Erp, W. et al. (2024). Deep brain stimulation of the central thalamus restores arousal and motivation in a zolpidem-responsive patient with akinetic mutism after severe brain injury. *Sci. Rep.* **14**:2950. DOI:https://doi.org/10.1038/s41598-024-52267-1.
25. Schiff, N.D., Giacino, J.T., Butson, C.R. et al. (2023). Thalamic deep brain stimulation in traumatic brain injury: a phase 1, randomized feasibility study. *Nat. Med.* **29**:3162–3174. DOI:https://doi.org/10.1038/s41591-023-02638-4.
26. Tasserie, J., Uhrig, L., Sitt, J.D. et al. (2022). Deep brain stimulation of the thalamus restores signatures of consciousness in a nonhuman primate model. *Sci. Adv.* **8**:eabl5547. DOI:https://doi.org/10.1126/sciadv.abl5547.
27. Zhang, Z., Huang, Y., Chen, X. et al. (2024). State-specific Regulation of Electrical Stimulation in the Intralaminar Thalamus of Macaque Monkeys: Network and Transcriptional Insights into Arousal. *Adv. Sci.* **11**:e2402718. DOI:https://doi.org/10.1002/advs.202402718.
28. Luppi, A.I., Uhrig, L., Tasserie, J. et al. (2024). Local orchestration of distributed functional patterns supporting loss and restoration of consciousness in the primate brain. *Nat. Commun.* **15**:2171. DOI:https://doi.org/10.1038/s41467-024-46382-w.
29. Kundu, B., Brock, A.A., Englot, D.J. et al. (2018). Deep brain stimulation for the treatment of disorders of consciousness and cognition in traumatic brain injury patients: a review. *Neurosurg. Focus* **45**:E14. DOI:https://doi.org/10.3171/2018.5.FOCUS18168.
30. Rezaei Haddad, A., Lythe, V. and Green, A.L. (2019). Deep brain stimulation for recovery of consciousness in minimally conscious patients after traumatic brain injury: a systematic review. *Neuromodulation* **22**:373–379. DOI:https://doi.org/10.1111/ner.12944.
31. Giacino, J.T., Kalmar, K. and Whyte, J. (2004). The JFK Coma Recovery Scale-Revised: Measurement characteristics and diagnostic utility. *Arch. Phys. Med. Rehabil.* **85**:2020–2029. DOI:https://doi.org/10.1016/j.apmr.2004.02.033.
32. Jennett, B. and Bond, M. (1975). Assessment of Outcome after Severe Brain-Damage - Practical Scale. *Lancet* **1**:480–484. DOI:https://doi.org/10.1016/s0140-6736(75)92830-5.
33. Song, M., Yang, Y., He, J. et al. (2018). Prognostication of chronic disorders of consciousness using brain functional networks and clinical characteristics. *Elife* **7**:e36173. DOI:https://doi.org/10.7554/eLife.36173.
34. Warren, A.E.L., Dalic, L.J., Thevathasan, W. et al. (2020). Targeting the centromedian thalamic nucleus for deep brain stimulation. *J. Neurol. Neurosurg. Psychiatry* **91**:339–349. DOI:https://doi.org/10.1136/jnnp-2019-322030.
35. Horn, A., Li, N., Dembek, T.A. et al. (2019). Lead-DBS v2: Towards a comprehensive pipeline for deep brain stimulation imaging. *Neuroimage* **184**:293–316. DOI:https://doi.org/10.1016/j.neuroimage.2018.08.068.
36. Avants, B.B., Tustison, N.J., Song, G. et al. (2011). A reproducible evaluation of ANTs similarity metric performance in brain image registration. *Neuroimage* **54**:2033–2044. DOI:https://doi.org/10.1016/j.neuroimage.2010.09.025.
37. Friston, K.J., Holmes, A.P., Worsley, K.J. et al. (1994). Statistical parametric maps in functional imaging: a general linear approach. *Hum. Brain Mapp.* **2**:189–210. DOI:https://doi.org/10.1002/hbm.460020402.
38. Schönecker, T., Kupsch, A., Kühn, A.A. et al. (2009). Automated Optimization of Subcortical Cerebral MR Imaging-Atlas Coregistration for Improved Postoperative Electrode Localization in Deep Brain Stimulation. *Am. J. Neuroradiol.* **30**:1914–1921. DOI:https://doi.org/10.3174/ajnr.A1741.
39. Ewert, S., Horn, A., Finkel, F. et al. (2019). Optimization and comparative evaluation of nonlinear deformation algorithms for atlas-based segmentation of DBS target nuclei. *Neuroimage* **184**:586–598. DOI:https://doi.org/10.1016/j.neuroimage.2018.09.061.
40. Vogel, D., Shah, A., Coste, J. et al. (2020). Anatomical brain structures normalization for deep brain stimulation in movement disorders. *Neuroimage. Clin.* **27**:102271. DOI:https://doi.org/10.1016/j.nicl.2020.102271.
41. Dang, Y., Wang, Y., Xia, X. et al. (2023). Deep brain stimulation improves electroencephalogram functional connectivity of patients with minimally conscious state. *CNS Neurosci. Ther.* **29**:344–353. DOI:https://doi.org/10.1111/cns.14009.
42. Krauth, A., Blanc, R., Poveda, A. et al. (2010). A mean three-dimensional atlas of the human thalamus: generation from multiple histological data. *Neuroimage* **49**:2053–2062. DOI:https://doi.org/10.1016/j.neuroimage.2009.10.042.
43. Chaure, F.J., Rey, H.G. and Quian Quiroga, R. (2018). A novel and fully automatic spike-sorting implementation with variable number of features. *J. Neurophysiol.* **120**:1859–1871. DOI:https://doi.org/10.1152/jn.00339.2018.
44. Oostenveld, R., Fries, P., Maris, E. et al. (2011). FieldTrip: Open source software for advanced analysis of MEG, EEG, and invasive electrophysiological data. *Comput. Intell. Neurosci.* **2011**:156869. DOI:https://doi.org/10.1155/2011/156869.
45. DeBusk, B.C., DeBruyn, E.J., Snider, R.K. et al. (1997). Stimulus-dependent modulation of spike burst length in cat striate cortical cells. *J. Neurophysiol.* **78**:199–213. DOI:https://doi.org/10.1152/jn.1997.78.1.199.
46. Richman, J.S. and Moorman, J.R. (2000). Physiological time-series analysis using approximate entropy and sample entropy. *Am J Physiol-Heart C* **278**:H2039–H2049. DOI:https://doi.org/10.1152/ajpheart.2000.278.6.H2039.
47. Lee, H., Wang, S. and Hudetz, A.G. (2020). State-Dependent Cortical Unit Activity Reflects Dynamic Brain State Transitions in Anesthesia. *J. Neurosci.* **40**:9440–9454. DOI:https://doi.org/10.1523/JNEUROSCI.0601-20.2020.
48. Liu, Q., Ma, L., Fan, S.Z. et al. (2018). Sample entropy analysis for the estimating depth of anaesthesia through human EEG signal at different levels of unconsciousness during surgeries. *PeerJ* **6**:e4817. DOI:https://doi.org/10.7717/peerj.4817.
49. Corrigan, B.W., Gulli, R.A., Doucet, G. et al. (2022). Distinct neural codes in primate hippocampus and lateral prefrontal cortex during associative learning in virtual environments. *Neuron* **110**:2155–2169.e4. DOI:https://doi.org/10.1016/j.neuron.2022.04.016.
50. Power, J.D., Schlaggar, B.L. and Petersen, S.E. (2015). Recent progress and outstanding issues in motion correction in resting state fMRI. *Neuroimage* **105**:536–551. DOI:https://doi.org/10.1016/j.neuroimage.2014.10.044.
51. Keuken, M.C., Bazin, P.-L., Crown, L. et al. (2014). Quantifying inter-individual anatomical variability in the subcortex using 7 T structural MRI. *Neuroimage* **94**:40–46. DOI:https://doi.org/10.1016/j.neuroimage.2014.03.032.
52. Zeidman, P., Jafarian, A., Corbin, N. et al. (2019). A guide to group effective connectivity analysis, part 1: First level analysis with DCM for fMRI. *Neuroimage* **200**:174–190. DOI:https://doi.org/10.1016/j.neuroimage.2019.06.031.
53. Friston, K.J., Kahan, J., Biswal, B. et al. (2014). A DCM for resting state fMRI. *Neuroimage* **94**:396–407. DOI:https://doi.org/10.1016/j.neuroimage.2013.12.009.
54. Zeidman, P., Jafarian, A., Seghier, M.L. et al. (2019). A guide to group effective connectivity analysis, part 2: Second level analysis with PEB. *Neuroimage* **200**:12–25. DOI:https://doi.org/10.1016/j.neuroimage.2019.06.032.
55. Yeh, F.C. and Tseng, W.Y.I. (2011). NTU-90: A high angular resolution brain atlas constructed by q-space diffeomorphic reconstruction. *Neuroimage* **58**:91–99. DOI:https://doi.org/10.1016/j.neuroimage.2011.06.021.
56. Glasser, M.F., Coalson, T.S., Robinson, E.C. et al. (2016). A multi-modal parcellation of human cerebral cortex. *Nature* **536**:171–178. DOI:https://doi.org/10.1038/nature18933.
57. Sun, H., Jiang, R., Dai, W. et al. (2023). Network controllability of structural connectomes in the neonatal brain. *Nat. Commun.* **14**:5820. DOI:https://doi.org/10.1038/s41467-023-41499-w.
58. Pedregosa, F., Varoquaux, G., Gramfort, A. et al. (2011). Scikit-learn: Machine Learning in Python. *J. Mach. Learn. Res.* **12**:2825–2830.
59. Kang, Y., Jamison, K., Jaywant, A. et al. (2022). Longitudinal alterations in gamma-aminobutyric acid (GABAA) receptor availability over ∼ 1 year following traumatic brain injury. *Brain Commun.* **4**:fcac159. DOI:https://doi.org/10.1093/braincomms/fcac159.
60. Sorokin, J.M., Davidson, T.J., Frechette, E. et al. (2017). Bidirectional Control of Generalized Epilepsy Networks via Rapid Real-Time Switching of Firing Mode. *Neuron* **93**:194–210. DOI:https://doi.org/10.1016/j.neuron.2016.11.026.
61. Demertzi, A., Antonopoulos, G., Heine, L. et al. (2015). Intrinsic functional connectivity differentiates minimally conscious from unresponsive patients. *Brain* **138**:2619–2631. DOI:https://doi.org/10.1093/brain/awv169.

62. Wu, X., Zou, Q., Hu, J. et al. (2015). Intrinsic Functional Connectivity Patterns Predict Consciousness Level and Recovery Outcome in Acquired Brain Injury. *J. Neurosci.* **35**:12932–12946. DOI:https://doi.org/10.1523/JNEUROSCI.0415-15.2015.
63. Vanhaudenhuyse, A., Noirhomme, Q., Tshibanda, L.J.F. et al. (2010). Default network connectivity reflects the level of consciousness in non-communicative brain-damaged patients. *Brain* **133**:161–171. DOI:https://doi.org/10.1093/brain/awp313.
64. Silva, S., De Pasquale, F., Vuillaume, C. et al. (2015). Disruption of posteromedial large-scale neural communication predicts recovery from coma. *Neurology* **85**:2036–2044. DOI:https://doi.org/10.1212/WNL.0000000000002196.
65. Boly, M., Phillips, C., Tshibanda, L. et al. (2008). Intrinsic brain activity in altered states of consciousness - How conscious is the default mode of brain function? *Ann Ny Acad Sci* **1129**:119–129. DOI:https://doi.org/10.1196/annals.1417.015.
66. Luppi, A.I., Craig, M.M., Pappas, I. et al. (2019). Consciousness-specific dynamic interactions of brain integration and functional diversity. *Nat. Commun.* **10**:4616. DOI:https://doi.org/10.1038/s41467-019-12658-9.
67. Qin, P., Wu, X., Huang, Z. et al. (2015). How Are Different Neural Networks Related to Consciousness? *Ann. Neurol.* **78**:594–605. DOI:https://doi.org/10.1002/ana.24479.
68. Northoff, G. and Heiss, W.D. (2015). Why Is the Distinction Between Neural Predispositions, Prerequisites, and Correlates of the Level of Consciousness Clinically Relevant? Functional Brain Imaging in Coma and Vegetative State. *Stroke* **46**:1147–1151. DOI:https://doi.org/10.1161/Strokeaha.114.007969.
69. Huang, Z., Zhang, J., Wu, J. et al. (2016). Decoupled temporal variability and signal synchronization of spontaneous brain activity in loss of consciousness: An fMRI study in anesthesia. *Neuroimage* **124**:693–703. DOI:https://doi.org/10.1016/j.neuroimage.2015.08.062.
70. Koike, T., Kan, S., Misaki, M. et al. (2011). Connectivity pattern changes in default-mode network with deep non-REM and REM sleep. *Neurosci. Res.* **69**:322–330. DOI:https://doi.org/10.1016/j.neures.2010.12.018.
71. Liu, X., Li, H., Luo, F. et al. (2015). Variation of the default mode network with altered alertness levels induced by propofol. *Neuropsych Dis Treat* **11**:2573–2581. DOI:https://doi.org/10.2147/Ndt.S88156.
72. Ilyas, A., Pizarro, D., Romeo, A.K. et al. (2019). The centromedian nucleus: Anatomy, physiology, and clinical implications. *J. Clin. Neurosci.* **63**:1–7. DOI:https://doi.org/10.1016/j.jocn.2019.01.050.
73. Sadikot, A.F. and Rymar, V.V. (2009). The primate centromedian-parafascicular complex: Anatomical organization with a note on neuromodulation. *Brain Res. Bull.* **78**:122–130. DOI:https://doi.org/10.1016/j.brainresbull.2008.09.016.
74. Benarroch, E.E. (2008). The midline and intralaminar thalamic nuclei: anatomic and functional specificity and implications in neurologic disease. *Neurology* **71**:944–949. DOI:https://doi.org/10.1212/01.wnl.0000326066.57313.13.
75. Harris, J.A., Mihalas, S., Hirokawa, K.E. et al. (2019). Hierarchical organization of cortical and thalamic connectivity. *Nature* **575**:195–202. DOI:https://doi.org/10.1038/s41586-019-1716-z.
76. Arnts, H., Coolen, S.E., Fernandes, F.W. et al. (2023). The intralaminar thalamus: a review of its role as a target in functional neurosurgery. *Brain Commun.* **5**:fcad003. DOI:https://doi.org/10.1093/braincomms/fcad003.
77. Mandelbaum, G., Taranda, J., Haynes, T.M. et al. (2019). Distinct cortical-thalamic-striatal circuits through the parafascicular nucleus. *Neuron* **102**:636–652.e7. DOI:https://doi.org/10.1016/j.neuron.2019.02.035.
78. Schiff, N.D. (2009). Central thalamic deep-brain stimulation in the severely injured brain: rationale and proposed mechanisms of action. *Ann. N. Y. Acad. Sci.* **1157**:101–116. DOI:https://doi.org/10.1111/j.1749-6632.2008.04123.x.

ACKNOWLEDGMENTS

We thank members of our laboratory for helpful comments on an earlier version of the manuscript and for helpful discussions. We thank Yang Qu for suggestions on our figure illustration in an earlier version. We thank Axel Krauth, Rémi Blanc, Alejandra Poveda, Daniel Jeanmonod, Anne Morel, and Gábor Székely at the University of Zurich and ETH Zurich for providing and approving the license for the Krauth/Morel thalamic atlas. Yan Yang was supported by funding from Beijing Natural Science Foundation grant Z210009; National Science and Technology Innovation 2030 Major Projects, STI2030-Major Projects grant 2022ZD0204800; National Natural Science Foundation of China grants 32070987 and 31722025; and Chinese Academy of Sciences Key Program of Frontier Sciences grant QYZDB-SSW-SMC019. H.W. and Y.H. were supported by funding from National Key R&D Program of China grant 2022YFB4700100 and Strategic Priority Research Program of Chinese Academy of Sciences XDB37030303. S.L. was funded as a chairholder from the Canada Excellence Research Chair in Neuroplasticity, as research director at the Belgian National Fund for Scientific Research, by the European Foundation of Biomedical Research, by the Foundation for Research and Rehabilitation of Neurodegenerative Diseases, and by National Natural Science Foundation of China 81920108023.

AUTHOR CONTRIBUTIONS

Conceptualization, Yan Yang and H.W.; methodology, Yan Yang and H.W.; investigation, H.W., Yan Yang, Y.H., P.Z., S.H., S.L., Y.D., Yi Yang, Q.G., L.X., X.X., and J.H.; clinical data resources, Y.D., Yi Yang, Q.G., L.X., X.X., and J.H.; formal analysis, H.W. and Y.H.; data curation, H.W., Yan Yang, and J.H.; visualization, H.W., Yan Yang, Y.H., and S.H.; funding acquisition, Yan Yang, H.W., and S.L.; project administration, Yan Yang; supervision, Yan Yang; writing – original draft, Yan Yang and H.W.; writing – review & editing, Yan Yang, H.W., Y.H., P.Z., S.H., S.L., and J.H.

DECLARATION OF INTERESTS

The authors declare no competing interests.

SUPPLEMENTAL INFORMATION

It can be found online at https://doi.org/10.1016/j.xinn.2025.100846.

LEAD CONTACT WEBSITE

Yan Yang, https://ibp.cas.cn/rc/yy/202411/t20241107_7435354.html.